Premature capacity (PCL) loss in Lead Acid batteries

Shedding and aging of the PbO_2 electrode

A research program carried out
at Battelle Geneva Switzerland
from 4/1977 to 4/1978

Part 1 to page 56

By
H.Giess
M.M Janssoone

SHEDDING AND AGING OF THE PbO_2 ELECTRODE

FINAL REPORT

FOR THE PERIOD 1st APRIL 1977 TO 30th APRIL 1978

by

H. GIESS, M.M. JANSSOONE

1. INTRODUCTION AND SUMMARY

This final report describes the results of the experiments carried out in the framework of the research program entitled:

"SHEDDING AND AGING OF THE PbO_2 ELECTRODE".

The research program was sponsored by a selected number of lead acid battery producer companies from Europe, the United States of America and Japan, and was carried out from the period of 1st April 1977 to 30th April 1978.

TABLE OF CONTENTS

page

The research program had the following objectives:

> *Description and quantification of the active mass disintegration phenomena occurring in a natural or accelerated way in the positive lead dioxide electrode when such an element is cyclically deeply discharged with or without an antimony-releasing current collector and with large active mass utilization factors.*
>
> *Elaboration of the ways in which this knowledge can be translated into practical prescription which will allow such degradation phenomena to be avoided.*

We have detected 4 distinct effects which antimony has on the cycling characteristics, namely:

- the effect on the specific active mass utilization;
- the effect on the random early failure rate;
- the effect on early failure with low density masses;
- the effect on accelerated aging;

and described the interaction of phenomena responsible for such effects and demonstrated that shedding is not the prime life-limiting factor with Sb-free electrodes.

Furthermore, by means of practical experiments and an exchange of know-how with the participating sponsor companies, we have developed and tested corrective actions which lessen the influence of the absence of Sb on the positive electrode. These corrective actions are:

(i) An improved curing technique to increase the active mass adhesion to the grid and reduce shrinkage fractures in the active mass-grid interface region.

(ii) The increase of the minimal apparent active mass density to ~4.0 $g \cdot ml^{-1}$ to achieve "satisfactory" cycle life.

(iii) The selection of a proper charging technique, i.e. current limited constant voltage charge, to be employed preferentially when the quality of the Sb-free electrode production cannot be kept at a very high standard.

In order to subject the electrodes to a wide range of conditions, we have made and employed materials and techniques which are also of a commercial nature or described in patents. This study should not be construed as a direct product comparison or an engineering evaluation nor instigate the abusive use of proprietary formulations protected by patents.

The results are presented below according to the evolution of the electrode life in following the sequence:

(a) Experimental details of electrode preparation and cycling.

(b) The effect of Sb during curing.

(c) The effect of Sb on the crystal habitus of PbO_2, its migration and localization in the active mass.

(d) The Sb^{I} effect.

(e) The Sb^{II} effect.

(f) The low-density-early-failure effect and the effect of H_3PO_4 additions.

(g) The Sb^{III} effect.

In conclusion of the work described below, it can be said that we have been able to refine the description of the beneficial effect of antimony and that the actions proposed for the preparation and utilization of Sb-free flat positive plates allow the possible introduction of maintenance-free traction batteries to be envisaged.

1.1. ABBREVIATIONS USED IN TEXT AND PICTURES

A certain amount of abbreviations were employed in this report in the place of lengthy, frequently used compound words. These terms were:

BG : Battelle-Geneva; indicates the place of electrode manufacture.

DELCO : DELCO-REMY, Division of General Motors; indicates a particular active mass preparation method and place of manufacture.

AM : Active Mass.

FCL : Formation Corrosion Layer; indicates the PbO_2 formed at the expense of the Pb of the grid during formation.

CCL : Cycling Corrosion Layer; indicates the PbO_2 formed at the expense of the Pb of the grid during cycling.

EOL : End of Life; indicates that the electrode has lost 50% of its capacity (100% is the 2nd cycle capacity).

Fully discharged: indicates that the electrode has reached, with the particular current +500 mV vs Hg/Hg_2SO_4, i.e. ~+1.6 V vs $Cd/CdSO_4$, i.e. ~+1.16 V vs H^+/H_2.

Sb^I : indicates the Sb^I effect, i.e. a modified specific active mass utilization ($Ah \cdot g^{-1}$) at a fixed electrode geometry and discharge current.

Sb^{II} : indicates the Sb^{II} effect, i.e. random early failures within 20 cycles with Sb-free electrodes.

Sb^{III} : indicates the Sb^{III} effect, i.e. the shorter cycle life in terms of cumulatively extracted $Ah \cdot g^{-1}$ before EOL.

LODEF : indicates the Low-Density Early Failure effect of Sb-free electrodes with active mass densities below 3.8 $g \cdot ml^{-1}$.

D.o.d.: Depth of discharge; indicates a different (normally higher) end-of-discharge-potential reached or lower active mass utilization achieved through modification of the discharge current or through H_3PO_4 additions.

S.E.M.: Scanning Electron Microscope.

XRMPS : X-Ray Microprobe Scan; indicates an analysis mode giving the elemental composition along a line and carried out with the scanning electron microscope in the electron microprobe mode.

XRMAS : X-Ray Microprobe Area Scan; indicates an analysis mode giving the elemental composition of a selected area and carried with the scanning electron microscope in the electron microprobe mode.

2. INSTRUMENTAL AND EXPERIMENTAL DETAILS

The following chapters outline the conditions of preparation and cycling of the positive electrodes and the ancillary equipment employed.

2.1. THE GRIDS

The most important variable in the investigation of the deep cycling behaviour of the positive electrode is the composition of the grid, i.e. the presence or absence of antimony. The selection of the type of the grid was dictated by major factors as:

(i) the availability of cast grids of different alloy compositions, but with identical dimensions and geometry;

(ii) the constraints imposed by the finite time available to accomplish a significant degradation of several consecutive sets of electrodes;

(iii) the achievement of a high active mass utilization factor ($K > 0.100$ Ah·g^{-1}) to maximize the phenomena relatable to the absence of antimony.

The selected grids were thus of the SLI-type, cast in an industrial environment by the following participating sponsors: SONNENSCHEIN (Ger.), PRESTOLITE-C&D (USA), TUDOR (Swe.) and GOULD (USA). The grids within the individual groups were of identical size and geometry and this allowed a straight forward comparison between the behaviour of Sb-containing and Sb-free grids. The uncertainity of comparing grids of varying sizes was thus eliminated.

2.1.1. DIMENSIONS OF GRIDS

The relative shapes and major dimensions are listed in Figure 1 and Table 1.

TABLE 1

GRID PRODUCER	TUDOR	SONNENSCHEIN	PRESTOLITE-C&D	GOULD
Grid width	~29 mm	~33.3 mm	~33.5 mm	~33.5 mm
Grid thickness	~1.0 mm	~ 1.7 mm	~ 1.5 mm	~ 1.8 mm
Grid weight (as shown)	~18.8 g	~22.4 g	~18.6 g	~21.1 g
Member-to-member distance	~2.5 mm	~ 2.8 mm	~ 3.5 mm	~ 3.5 mm

2.1.2. GRID ALLOY COMPOSITION

The grid alloys were of the following compositions:

SONNENSCHEIN: Nominal composition 7 Sb - 4.5 Sb - 2.7 Sb - CaSn

TABLE 2

7 Sb	6.30% Sb	0.011% Sn	0.077% As	0.002% Cd	0.002% Ag	0.033% Cu
4.5 Sb	4.54% Sb	0.011% Sn	0.066% As	0.004% Cd	0.004% Ag	0.049% Cu
2.7 Sb	2.95% Sb	0.093% Sn	0.062% As	0.004% Cd	0.004% Ag	0.053% Cu
CaSn	0.075% Ca	0.57 % Sn	n.a.	n.a.	n.a.	n.a.

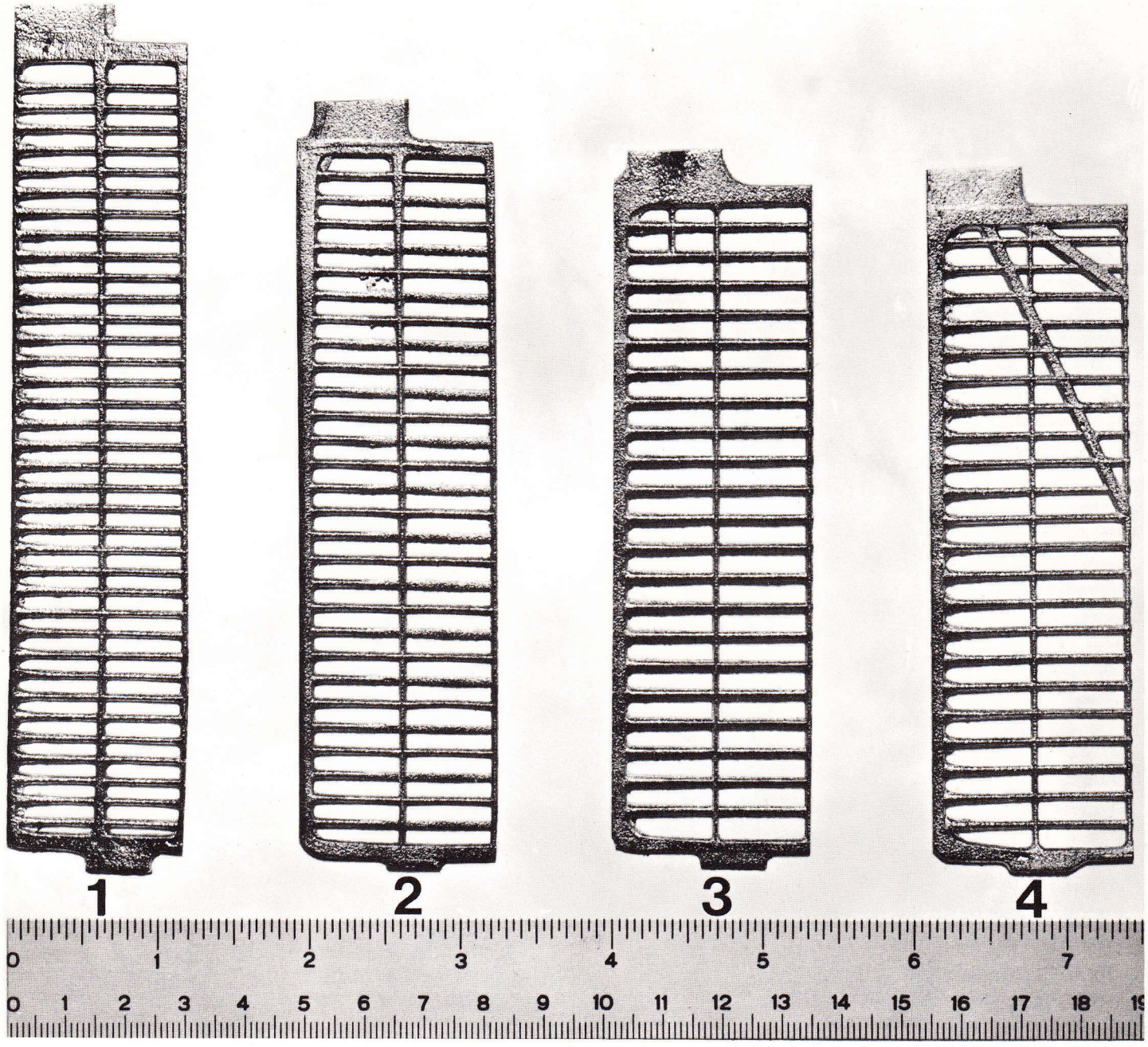

Fig. 1 Grids.

1 : TUDOR (Swe) - Sn-ASTAG.
2 : SONNENSCHEIN (Ger) - 7 Sb, 4.5 Sb, 2.7 Sb, CaSn.
3 : PRESTOLITE-C&D (USA) - 5 Sb, 3.3 Sb, CaSn.
4 : GOULD (USA) - CdSb.

PRESTOLITE-C&D: Nominal composition 5 Sb - 3 Sb - CaSn

TABLE 3

5 Sb	4.46% Sb	0.15% Sn	0.16% As	0.001% Cd	0.003% Ag	0.036% Cu
3 Sb	3.15% Sb	0.34% Sn	0.58% As	0.05 % Cd	0.003% Ag	0.080% Cu
CaSn	0.102% Ca	0.78% Sn	n.a.	n.a.	n.a.	n.a.

TUDOR: Nominal composition Sn-ASTAG

TABLE 4

Sn-ASTAG	0.6% Sn	0.1% Te + As + Ag	n.a.

GOULD: Nominal composition CdSb

TABLE 5

CdSb	1.33% Sb	1.44% Cd	0.006% As	0.001% Sn

2.1.3. ANCILLARY PREPARATIONS

The grid portions for the cycling tests were cut from the standard grids and provided with a 2 mm Ø pure lead wire current collector welded to the collector tab. Before pasting, the grids were ultrasonically degreased and cleaned in an acetone-pentane mixture.

A certain amount of CaSn grids were additionally treated with a steel wire brush in order to eliminate possible surface oxides and mold coating residues. Moreover, this treatment was intended to produce a surface with a worked structure similar to rolled and expanded metal CaSn grids. This treatment showed, however, no appreciable influence on the subsequent cycling behaviour.

The additional surface treatment like coating with gold or cadmium was carried out with standard electroplating techniques. The 1.5 µm antimony coating deposited on certain sets of CaSn grids was produced by a displacement technique according to US Patent 3.933.524 (1976). The appropriate solution for a good adhering layer was found to require the following composition: 2200 ml HBF_4 (40%, d = 1.31) + 132 g Sb_2O_3 + 67 g HF (50%) (filter to a clear solution and immerge the degreased and etched grids for ~20 - 25 seconds). The thickness of the Sb coating was determined by direct measurements on metallographic cross-sections.

2.1.4. METALLURGICAL STRUCTURE OF THE GRID

The metallurgical structure of the grids is relevant for the rate of release of antimony and for the eventual "buckling" of the plate due to preferential grain boundary attack. The microdistribution of antimony is important as the surface segregation and continuity of the β-phase (Sb-rich) influence the local availability of antimony.

Surface segregation, i.e., inverse segregation gives an abnormal large source of antimony on the surface of the grid and this antimony, available during curing and as soluble species during the first moments of formation, strongly influences active mass adhesion in a proportionally larger degree than expected from the single analytical composition of the grid.

Continuity of the β-phase crystals. The main source of Sb during the corrosion process is the β-phase crystallite. If these crystallites are continuous and intercept the grid surface or corrosion front in sufficient numbers, then the presence of areas of metallic Sb or a steady flow of Sb ions is assured. When, due to thermal treatments or other factors, these crystallites are broken into fragments or do not intercept the grid surface in sufficient numbers, then the metallic Sb surfaces and massive Sb ion generation is impaired with consequences on the bond quality active mass-grid.

The observed microstructures, representative of the portion of the grid employed, are shown in Figures 2 to 19.

Sb alloys

The nominal 7 Sb, 4.5 Sb and 5 Sb alloys show marked accumulation of Sb crystals on the surface due to inverse segregation.

This phenomena is not observed in the nominal 3.3 Sb, 2.7 Sb and Cd-Sb alloys.

Sb-free alloys

The CaSn (SONNENSCHEIN) grid shows the typical grain structure with a dendritic substructure given by the addition of tin to the alloy. Small precipitations at boundary nodes were also observed. In the CaSn (PRESTOLITE) grids, the grain structure is finer, showing serrated grain boundaries, minimal dendritic substructure and indications of recrystallization and precipitation phenomena behind the migrated internal boundaries.

The Sn-ASTAG alloy shows a grain structure with dendrites and precipitation of a secondary phase.

Metallurgical structures

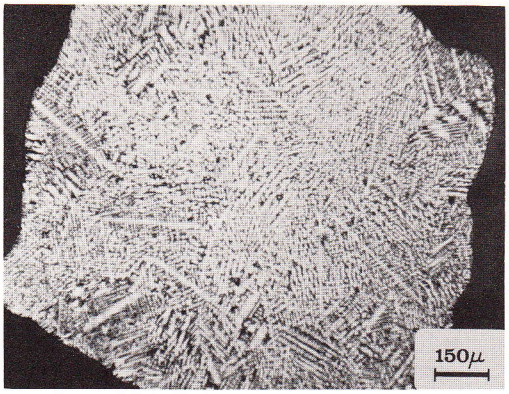

Fig. 2 7 Sb - SONNENSCHEIN.

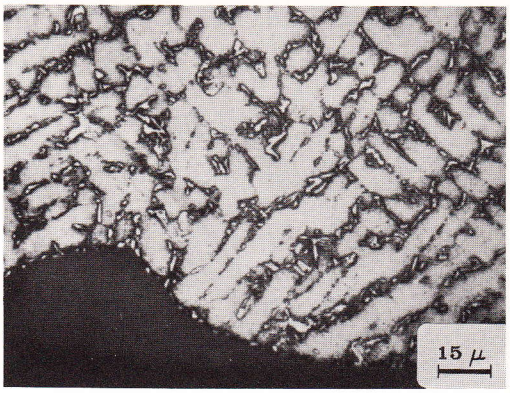

Fig. 3 Detail showing surface Sb.

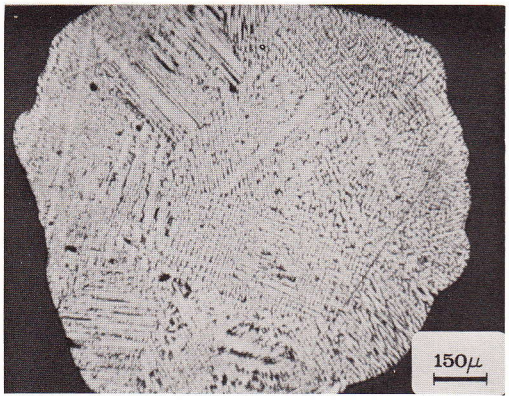

Fig. 4 4.5 Sb - SONNENSCHEIN.

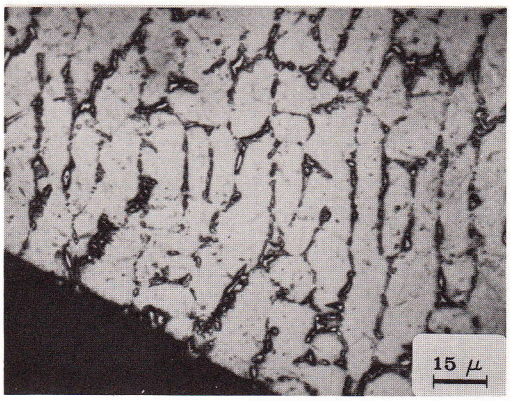

Fig. 5 Detail showing surface Sb.

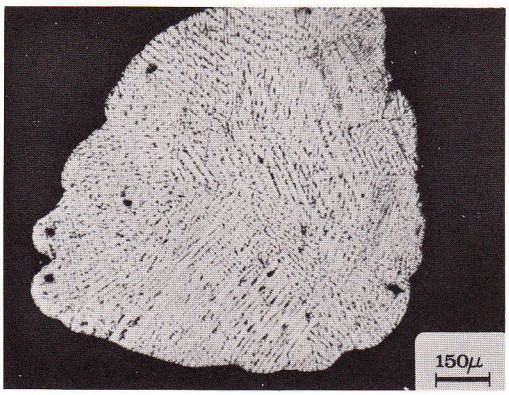

Fig. 6 2.7 Sb - SONNENSCHEIN.

Fig. 7 Detail showing surface Sb.

Metallurgical structures

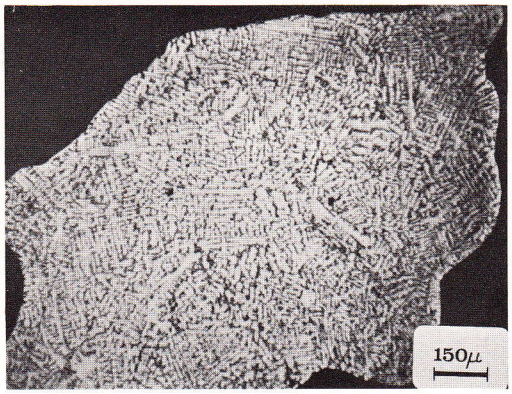

Fig. 8 5 Sb - PRESTOLITE-C&D.

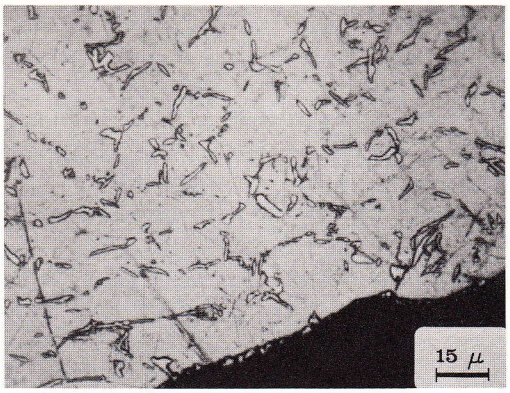

Fig. 9 Detail showing surface Sb.

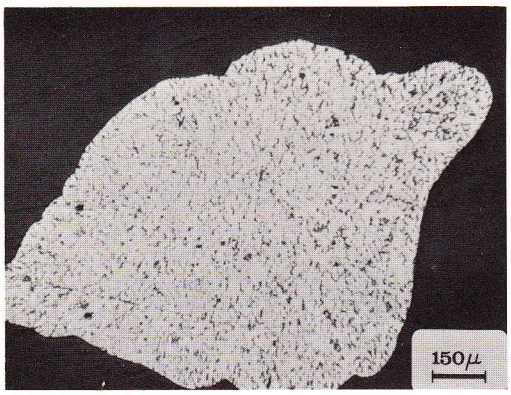

Fig. 10 3.3 Sb - PRESTOLITE-C&D.

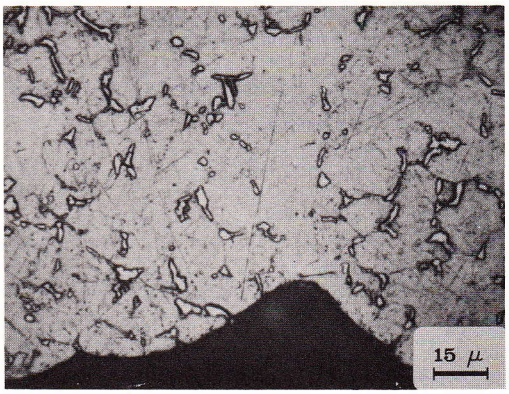

Fig. 11 Detail showing surface Sb.

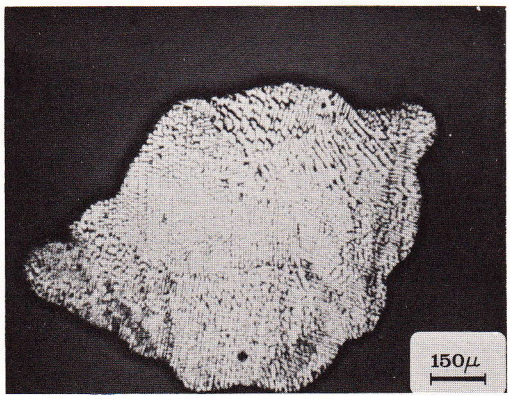

Fig. 12 CdSb - GOULD.

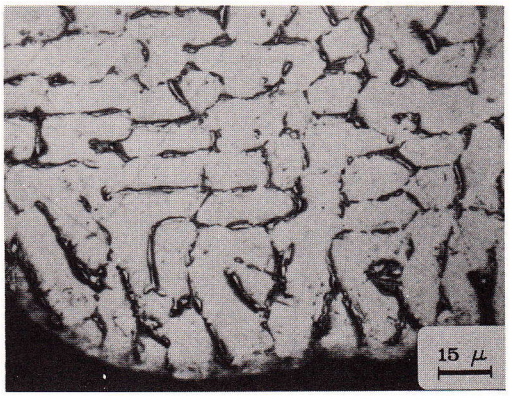

Fig. 13 Detail showing surface Sb.

Metallurgical structures

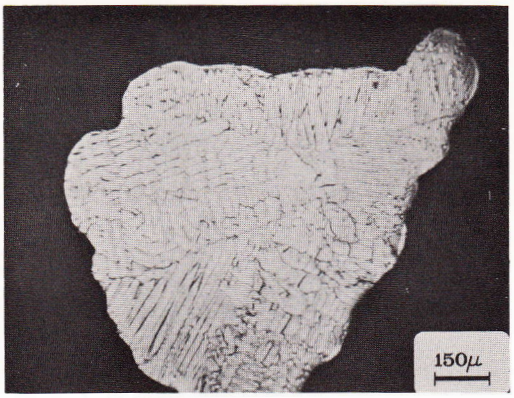

Fig. 14 CaSn - SONNENSCHEIN.

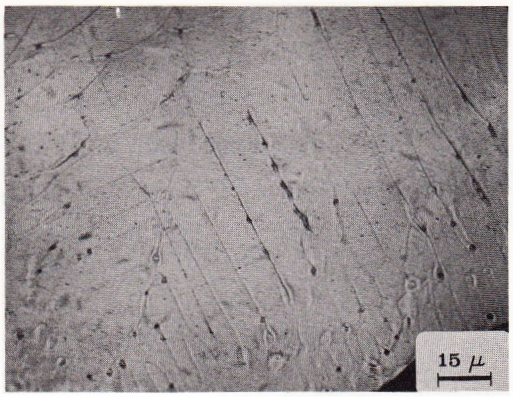

Fig. 15 Detail showing substructure.

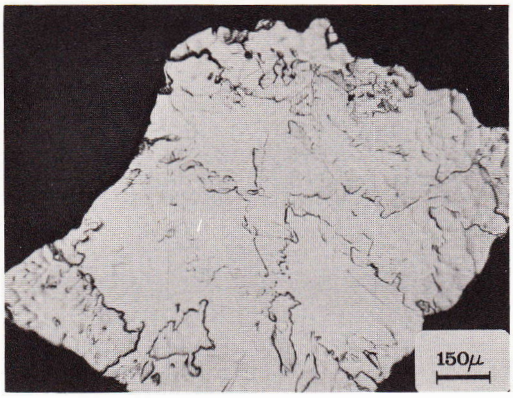

Fig. 16 CaSn - PRESTOLITE C&D.

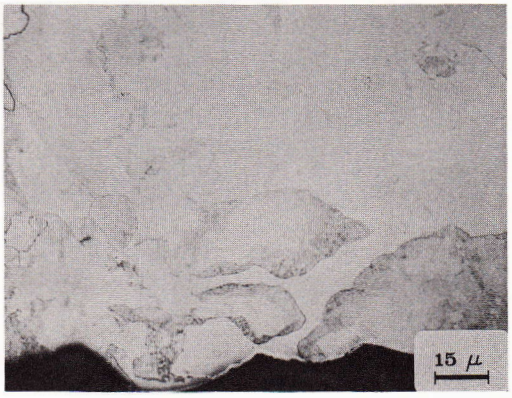

Fig. 17 Detail showing substructure.

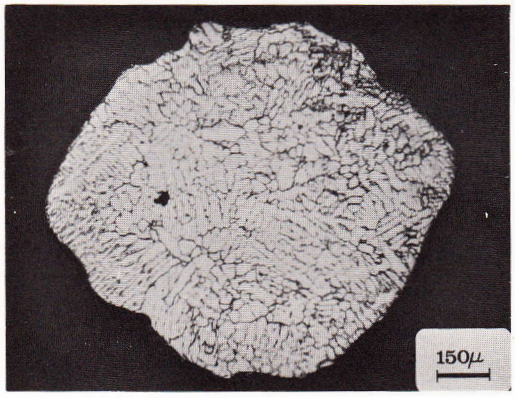

Fig. 18 Sn-ASTAG - TUDOR.

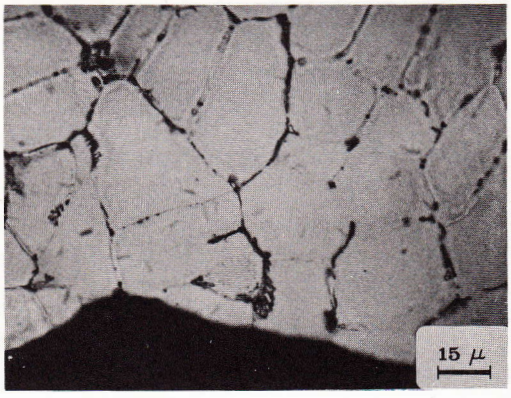

Fig. 19 Detail showing substructure.

2.2. POSITIVE ELECTRODE PREPARATION

2.2.1. OXIDES

The oxides employed for the positive paste preparation consisted of Ball-mill and Barton-pot oxides delivered by W. HAGEN (Ger.) and R. BOSCH (Ger.), respectively.
The set of electrodes pasted by DELCO-GM (USA) employed Barton-pot oxides.

Ball-mill oxide

12 of 13 paste batches prepared for the positive test electrodes were made from one batch of oxide freshly prepared and delivered in June 1977 and employed through February 1978. The intrinsic aging of the oxide was noticeable in the subsequent performance of the electrodes. The 13th paste was prepared again from a fresh oxide batch and the experienced performance, in terms of reduced failures of CaSn electrodes, was good and comparable to that recorded with the initial paste batches of the first oxide delivery (see discussion of the behaviour of electrodes during curing).

Barton oxide

A single batch of paste (13 B) from the freshly prepared Barton-pot oxide was made at Battelle-Geneva with results, in terms of failure of CaSn electrodes, comparable to that of batches prepared with "fresh" ball mill oxide.

Table 6 shows the analysis of the oxides carried out according to standard procedures in collaboration with the quality control laboratories of R. BOSCH (Ger.) and DELCO-GM (USA).

TABLE 6

1st BATCH BALL-MILL OXIDE (W. HAGEN) on delivery (1st paste batch) : ~30% free Pb at the end (12th paste batch) : 18% free Pb - 82% PbO - 245 $mg \cdot g^{-1}$ acid absorption, 1.97 $g \cdot ml^{-1}$ apparent density
2nd BATCH BALL-MILL OXIDE (W. HAGEN) on delivery (13 A paste batch) : 34% free Pb - 66% PbO - 230 $mg \cdot g^{-1}$ acid absorption, 2.13 $g \cdot ml^{-1}$ apparent density
1st BATCH BARTON-POT OXIDE (R. BOSCH) on delivery (13 B paste batch) : 9% free Pb - 91% PbO - 253 $mg \cdot g^{-1}$ acid absorption, 1.83 $g \cdot ml^{-1}$ apparent density
BARTON-POT OXIDE employed for set DELCO-1 : 20% free Pb DELCO-2 : 22% free Pb DELCO-3 : ~20% free Pb (n.a.)

2.2.2. PASTE PREPARATION

The positive paste was prepared in order to achieve a good deep cycling performance with the following proportion (Table 7) of raw materials kept constant in all the batches:

TABLE 7

8.000 kg oxide	1000	82.4% w/w
0.960 kg H_2O	120	9.8% w/w
0.756 kg H_2SO_4 (d = 1.42; 319 g SO_3)	95	7.8% w/w
0.0048 kg polypropylene fibres (3 den/3 mm)	0.0006	

This gave a paste with 3.3% SO_3 wet and 2.9% SO_3 dry. The mixing sequence employing a "Sigma" mixer was the following (Table 8):

TABLE 8

5 min	- mixing of the dry oxide - addition of 0.700 kg H_2O (72%)
5 min	- mixing of the wetted oxide - addition under constant mixing action and at temperatures between 55° - 70°C of 0.756 kg H_2SO_4 with a rate of approximately 84 g/min
5 min	- mixing of the reacted oxide - addition of 0.260 kg H_2O (28%) - mixing till a temperature of 41 - 42°C was reached

The density of the wet paste at the end of mixing was approximately between 4.4 and 4.2 $g \cdot ml^{-1}$, depending on the free lead content of the ball-mill oxide.

The single Barton-pot oxide batch gave a wet density of 4.4 $g \cdot ml^{-1}$.

The loss of water during the curing and drying was approximately 10 - 11% giving a final apparent dry density of the paste of 3.8 to 4.0 $g \cdot ml^{-1}$. Free lead amounted to less than 2%.

Other paste preparations (DELCO-1 - 2 - 3)

Three paste preparations and related curing have been carried out by DELCO-GM (Anderson/USA) in order to test the behaviour of tetrabasic, low density masses and improved active mass-grid bonding.

The paste preparation was based on a Barton-pot oxide and 1.40 $g \cdot ml^{-1}$ H_2SO_4 and gave the following results:

TABLE 9

DELCO-1 :	3.85 $g \cdot ml^{-1}$ wet density (63.1 g/cu·in) Water loss during curing and drying: ~12% of original weight. $PbSO_4$: 13.35%; free Pb : 0.067% (no Dynel)
DELCO-2 :	3.53 $g \cdot ml^{-1}$ wet density (57.8 g/cu.in) Water loss during curing and drying: ~13% $PbSO_4$: 14.3% ; free Pb : 0.28% (Dynel)
DELCO-3 :	4.20 $g \cdot ml^{-1}$ wet density (69 g/cu·in) Water loss during curing and drying: ~10% $PbSO_4$: 10.3% ; free Pb : 0.40% (Dynel)

14% $PbSO_4$ = 3.7% SO_3 % $PbSO_4$ / 3.8 = % SO_3

The loss of water experienced with these paste formulations (10 to 13%) gave a final corrected apparent density, before formation, of

DELCO-1	3.39 $g \cdot ml^{-1}$
DELCO-2	3.07 $g \cdot ml^{-1}$
DELCO-3	3.78 $g \cdot ml^{-1}$

Mixtures of active mass with antimony sources

A certain number of electrodes were prepared with active mass formulations containing antimony metal powder, tin metal powder and PbSb (2%) metal powder with a mean grain size of ~30 µm.

These elements were added in a concentration of 0.2% w/w to the wet paste at the end of the paste mixing sequence and the mixture homogenized with an additional mixing period.

2.2.3. PASTING

The electrodes of all the test sets were handpasted with preweighed amounts of wet paste. This amount of paste was constant within a grid type throughout the entire research program and kept independent of the density fluctuation of the paste (Table 10).

TABLE 10

Grids type SONNENSCHEIN Grids type TUDOR	22.0 g wet paste - BG
Grids type PRESTOLITE-C&D GOULD	20.0 g wet paste - BG
Grids type SONNENSCHEIN DELCO-paste	DELCO-1 : 19.5 g wet paste DELCO-2 : 18.4 g wet paste DELCO-3 : 22.3 g wet paste

The electrodes were pasted on both sides and "overpasting" of the horizontal grid members was deliberately intended.

Particular attention has been paid to equally distribute the mass in the grid frame. The pasted electrodes were immediately stored vertically, separated by a 4 mm air gap in the curing vessel at room temperature (25°C) and 100% relative humidity in order to eliminate crack formation and shrinkage of the active mass as much as possible.

2.2.4. CURING

The curing procedure adopted consisted of the following sequence of temperatures and relative humidities and gave a tribasic lead sulfate mass:

48 hours at 45°C and 100% relative humidity (I)

24 hours at 55°C and 100% relative humidity (II)

18 hours at 55°C and 20% relative humidity (III).

As we will later discuss, the electrodes showed varying amounts of shrinkage fractures in the region near the horizontal grid member at the end of the curing period II.

The curing process employed in the preparation of the sets DELCO-1 - 2 - 3 is a proprietary procedure and has been carried out by DELCO-GM. It basically consists in a high temperature curing process to transform the initial PbO + $3PbO \cdot PbSO_4 \cdot nH_2O$ mixture in situ in the electrode into a PbO + $4PbO \cdot PbSO_4$ mixture. This treatment achieves excellent bonding of the active mass to the grid and totally eliminates shrinkage fractures in the active mass.

2.2.5. FORMATION

The formation of the positive electrodes was carried out in separate formation containers at 40°C with an excess of 1.06 sp.gr. H_2SO_4 (630 ml/electrode) against lead sheet negatives. These lead sheet negatives were changed when necessary in order to avoid a build up of antimony in the formation cell.

The formation sequence adopted provided an over-formation in order to insure complete transformation of the oxides and sulfates to PbO_2. An initial step with a low current density was introduced in order to avoid unduly stressing the interface grid-active mass.

TABLE 11

Formation sequence for		
SONNENSCHEIN type grids	~20 g	dry active mass
DELCO-3 set	~20 g	dry active mass
TUDOR type grids	~20 g	dry active mass

1 hour soaking in 1.06 sp.gr. H_2SO_4 at 40°C

3 hours	208 mA/electrode	10.4 mA/g mass	=	0.624 Ah
15.5 hours	417 mA/electrode	20.8 mA/g mass	=	6.463 Ah
8 hours	280 mA/electrode	14.0 mA/g mass	=	2.240 Ah
16 hours	141 mA/electrode	7.0 mA/g mass	=	2.256 Ah

total formation current input	:	11.583 Ah
specific formation current input	:	0.579 $Ah.g^{-1}$ (theoretical 0.224 Ah)
formation factor	:	2.58

TABLE 12

Formation sequence for		
PRESTOLITE type grids	~18 g	dry active mass
GOULD type grids	~18 g	dry active mass
DELCO-1 and -2 sets	~17 - 15 g	dry active mass

1 hour soaking in 1.06 sp.gr. H_2SO_4 at 40°C

3 hours	187 mA/electrode	10.4 mA/g mass	=	0.561 Ah
15.5 hours	375 mA/electrode	20.8 mA/g mass	=	5.625 Ah
8 hours	252 mA/electrode	14.0 mA/g mass	=	2.016 Ah
16 hours	127 mA/electrode	7.0 mA/g mass	=	2.032 Ah

total formation current input	:	10.234 Ah
specific formation current input	:	0.569 $Ah.g^{-1}$ (theoretical 0.224 Ah)
formation factor	:	2.54

The electrodes are damp dried with Kleenex tissue paper and assembled within 1 hour into complete cells.

2.3. THE POSITIVE-NEGATIVE ELECTRODE - SEPARATOR ASSEMBLY

The positive electrode was assembled into a cell with two electrochemically oversized negatives. These negatives were cut from antimony-free ASTAG electrodes, produced and delivered drycharged by TUDOR (Swe.). The separator consisted of two microporous rubber separators of the type ACE-SIL-200 of AMERACE (USA). These separators were in unrestrained contact with the positive electrode through their ribs. These ribs rested

(a) on the center vertical grid member

and

(b) on the active mass toward the edge of the electrode.

See also Figs. 20 and 21. The active mass was free to expand into the cavities of the separator and to sediment on the bottom of the cell.

2.3.1. THE TEST CELL

The 200 test cells for the electrode cycling tests were machined from Plexiglass (cast quality) which allowed a substantially chlorine-free construction and the visual observation of the electrode assembly. See also Fig. 22.

The shedded positive mass was collected in the appropriate mud collection volume on the bottom of the cell. As the positive electrode was resting on a thin bridge above the mud volume, the shedded material did not have any electrical contact with the electrode. The negative mud was completely retained by the appro-

Separator-grid assembly

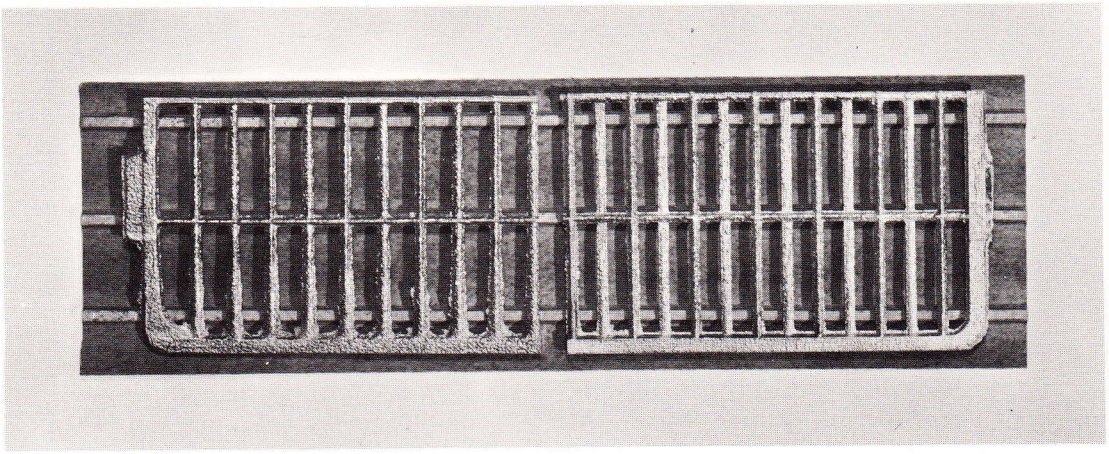

Fig. 20 Rib position of the separator in the assembled cell.

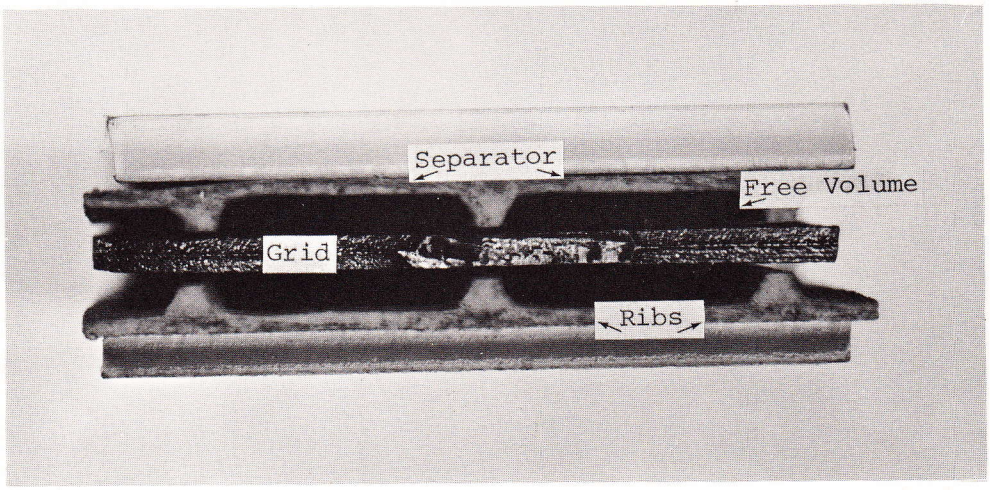

Fig. 21 Free volume for active mass expansion and shedding.

priate design of the negative electrode-separator support of the cell (see Fig. 22, Pos. A). The mud was extracted periodically as needed by unscrewing the viton-Oring sealed plug and flushing the sediment onto a filter membrane for washing, drying and weighing. The collected electrolyte was reintroduced into the cell.

The separators were lodged loose into recesses in the cell wall in order to fix their position and their degree of movement and prevent through a simple labyrinth seal any dendrite short-circuiting.

The amount of acid in the cell was limited in order to duplicate real cell behaviour (50 ml 1.285 sp.gr H_2SO_4 - 25°C). Each cell was provided with a Hg/Hg_2SO_4 reference electrode kept within a separate constant acid-strength (d = 1.285) volume. Two 1 mm Ø holes plugged substantially acid tight with silica threads, acted as Luggin capillary probes "looking" in a constant geometrical arrangement toward two locations on the edge of the positive plate (~0.5 mm distance probe tip - grid).

2.4. THE ELECTRODE CYCLING EQUIPMENT

The cycling equipment consists basically in 168 constant current charge-discharge units complemented by 24 similar modules for constant voltage (or potential) charge-constant current discharge.

The cycling units for the present research program were employed in the following mode:

(i) the discharge of the individual cells to an individually settable positive electrode potential or cell voltage, i.e. to +500 mV vs Hg/Hg_2SO_4;

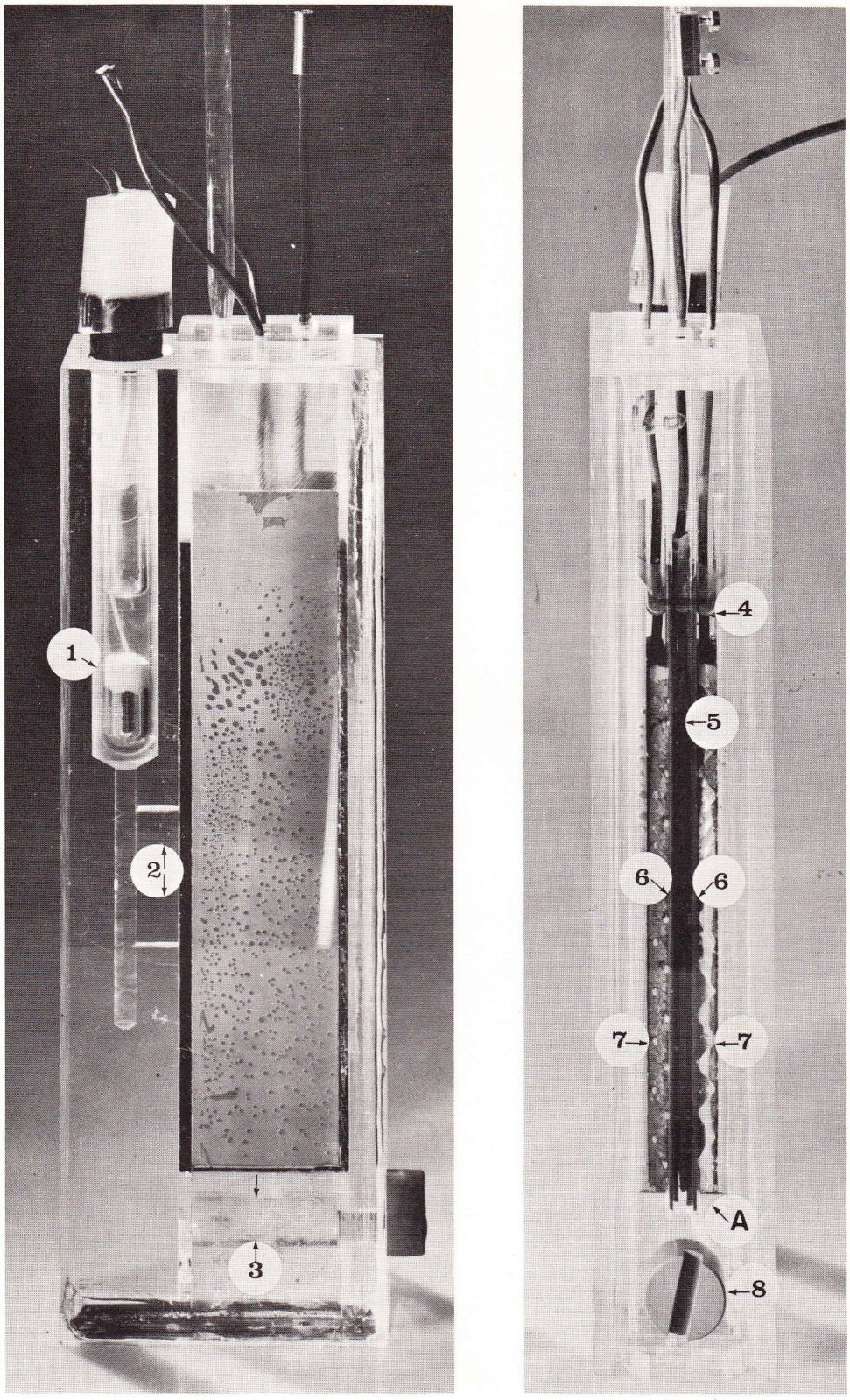

Fig. 22 Test cell.

1) Hg/Hg_2SO_4 reference electrode
2) Luggin capillary probes
3) Mud collection volume
4) Electrolyte level
5) Positive electrode
6) Separators
7) Negative electrodes
8) Plug for mud extraction

A) Negative-separator geometry for negative mud retention.

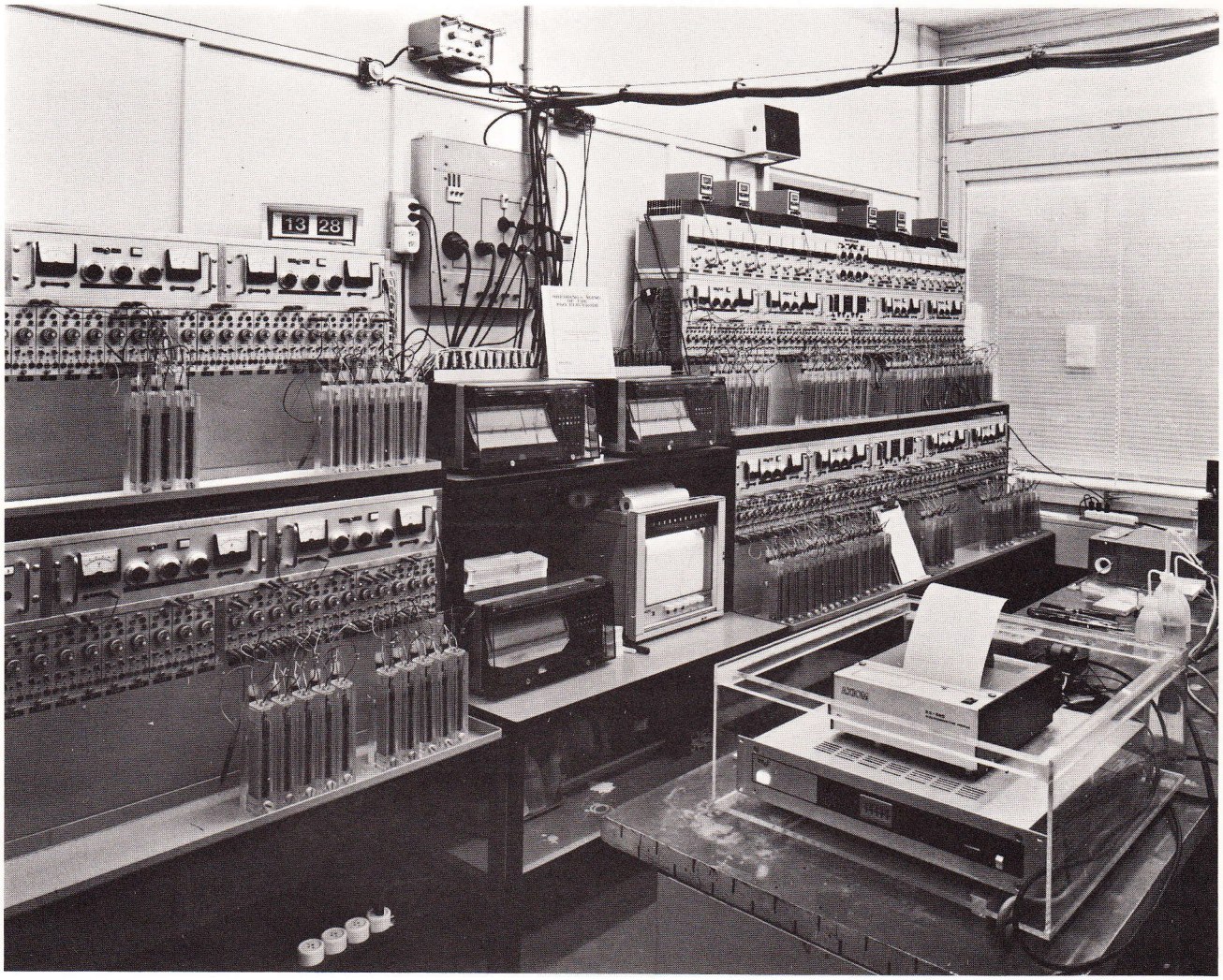

Fig. 23 Test room with cycling unit.

(ii) the recording for each cell and each discharge of the elapsed discharge time from the start of the discharge till the particular potential limit was reached.

This was achieved within a ± 0.001 hour precision with a simple microcomputer system built around an INTEL-8080 microprocessor, incorporating a Battelle-Geneva developed matrix scanner and related print-out;

(iii) the two-step constant current charge for respectively 3 and 4 hours (C_1 and C_2) with the charging current identical for a minimum of 12 identical samples or alternatively;

(iv) the constant voltage charge individually settable for each cell with a maximum current limitation;

(v) the record of selected potential vs time curves and, in case of constant voltage charging, the integration of the amount of charge within ± 1 mAh precision.

Figure 23 shows the test room with the assembly of the above described units with the micro-computer and printer in front and the 4 12-channel potential recorders and part of the cycling units in the rear.

The cycling room was kept at 25°C ± 1 with a relative humidity of 60 - 75% to reduce electrolyte evaporation.

2.5. THE CYCLING REGIME

The cycling regime chosen for the aging of the positive electrode consisted in a deep discharge-shallow overcharge sequence at $25^{o} \pm 1^{o}C$.

The basic parameters which remained constant during the research program are shown in Tables 13, 14 and 15.

TABLE 13

Electrodes with 20 g/dry active mass (SONNENSCHEIN-TUDOR-DELCO-3)	
Acid volume	: 50 ml 1.285 sp.gr. H_2SO_4
Acid/active mass ratio	: 2.5 $ml \cdot g^{-1}$
Discharge current	: 600 mA·electrode (constant over life)
Specific discharge current	: 30 $mA \cdot g^{-1}$ active mass
Discharge duration	: ~4 hours (decreasing)
Minimum potential at end of discharge	: +500 mV vs Hg/Hg_2SO_4 in 1.285 sp.gr. H_2SO_4
Open circuit stand after discharge	: 5 hours minus the discharge period
Charge current:	
. 1st period of 3 hours	: 600 mA·electrode
. 2nd period of 4 hours	: adapted to give ~18 - 20% overcharge
The current of the 2nd charging period was adjusted periodically to give the appropriate amount of overcharge	

TABLE 14

Electrodes with 18 g/dry active mass (PRESTOLITE-GOULD-DELCO-1 + 2)	
Acid volume	: 50 ml 1.285 sp.gr. H_2SO_4
Acid/active mass ratio	: 2.78 $ml \cdot g^{-1}$
Discharge current	: 480 mA·electrode (constant over life)
Specific discharge current	: ~26.7 $mA \cdot g^{-1}$ active mass
Discharge duration	: ~4 hours (decreasing)
Minimum potential at end of discharge	: +500 mV vs $Hg/HgSO_4$ in 1.285 sp.gr. H_2SO_4
Open circuit stand after discharge	: 5 h minus the discharge period
Charge current:	
. 1st period of 3 hours	: 480 mA·electrode
. 2nd period of 4 hours	: adapted to give 18 - 20% overcharge
The current of the 2nd charging period was adjusted periodically to give the appropriate amount of overcharge.	

A certain set of electrodes was cycled under a constant current discharge-constant voltage charge regime with the following parameters (Table 15).

TABLE 15

- Discharge current	: 600 mA/500 mA
- Discharge duration	: ~4 hours (decreasing)
- Minimum voltage at end of discharge	: 1.560 Volt
(NB: the overdimensioned negatives did not contribute significantly to the decreased voltage at the end of discharge)	
- Potential of the positive electrode at 1.560 Volt cell voltage	: ~+500 - +520 mV vs Hg/Hg_2SO_4 in 1.285 sp.gr. H_2SO_4
Open circuit stand after discharge	: 5 h minus discharge period
1st charge voltage; cycle 1 to cycle 15	: 2.405 Volt ; +25°C
- Maximum allowed current	: 600 mA/500 mA
- Overcharge	: ~4 - 7%
- Potential of positive electrode at end of charge	: ~+1340 - +1360 mV vs Hg/Hg_2SO_4
- Maximum potential of positive electrode at 2.405 V cell voltage	: ~+1360 - +1370 mV vs Hg/Hg_2SO_4

The above selected cell voltage and resulting overcharge did not allow a satisfactory charging regime to be run. This was caused by the strong polarization of the negative electrode (Sb-free) which markedly influenced the total final current flow and the potential of the positive electrode.

24 a

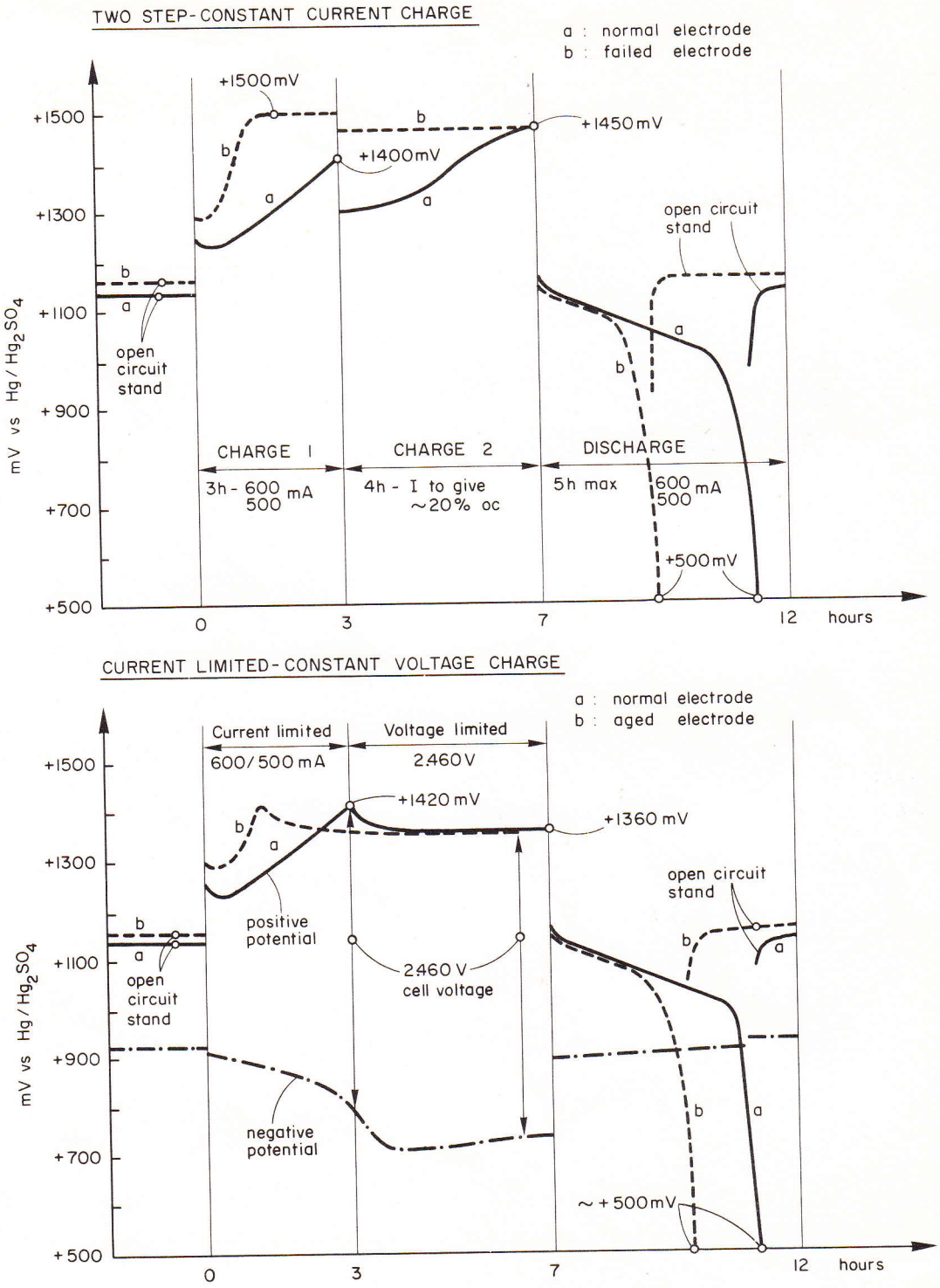

Fig. 24 Potential vs time curves with constant current and current limited constant voltage charge.

From the 16th charge cycle, a new voltage limit was imposed:

TABLE 16

Charge voltage cycle 16 to EOL	: 2.460 Volt ; 25°C
- Maximum allowed current	: 600 mA/500 mA
- Overcharge	: ~8 - 9%
- Potential of positive electrode at end of charge	: ~+1360 mV
- Maximum potential of positive electrode at 2.460 Volt cell voltage	: +1410 mV - 1415 mV vs Hg/Hg_2SO_4 shifting gradualy to +1430 mV

Typical potential vs time curves are shown in Fig. 24.

2.6. SAMPLE SIZE

To assure the validity of the observed phenomena, replicate samples were put on test. In critical experiments, 12 identical samples served as replicates whereas with less critical ones 4 to 6 replicates were judged sufficient.

The particular arrangement of our cycling unit allowed our electrodes to be discharged to the selected +500 mV vs Hg/Hg_2SO_4 discharge stop as 12 individual entities,whereas under charge these 12 electrodes were treated as a single unit.

In the majority of the cases, the discharge capacity of the electrodes was very similar, i.e. $\pm$ 2 - 3%, but in cases of random early failure, the failing samples were submitted to a proportionally higher charge Ah input. This charge input was tailored to give 20% overcharge in relation to the mean of the "good" samples and therefore resulted in a much larger overcharge with failing low capacity electrodes.

3. EXPERIMENTAL RESULTS

3.1. INTRODUCTION

The work program carried out between April 1977 and April 1978 was based on a step-by-step, comparative investigation of antimony-containing and antimony-free positive plates under a deep cycling regime. The information shown in the following chapters present the investigative results obtained in order to answer the following questions as completely as possible:

Is antimony needed to obtain a satisfactory deep cycling behaviour?

If yes,

- *when in the preparation and cycle history of the electrode?*
- *where in terms of specific action?*
- *how much in terms of minimal concentration required in the grid and/or in the active mass?*
- *what are the substitutes and technological requirements for a satisfactory cycle life of Sb-free electrodes?*

We will present the results split into several interrelated investigations emphasizing the observed differences between an Sb-free and an Sb-containing positive electrode, analyzing the failure mode(s) and presenting the results obtained with experiments designed to elucidate the exact mechanism of the action of antimony.

These investigative analyses and related experiments were designed to give an answer as clear as possible, but due to the intrinsic complexity and interrelation of the parameters in the positive electrodes, a yes/no situation was not always possible.

We understand from discussions with our sponsors that in-house work has led to progress in tackling the practical problems of antimony-free electrodes and that certain answers crystallized from experimental work on how antimony acts.

We do not think that our experimental data conflict with this information and these methods of preparation, although the following analyses and conclusions might differ to a certain extent from those made by the sponsoring companies.

We will therefore emphasize in detail how these data were obtained. Furthermore, due to the fact that we could not pursue every alternative within the financial and time scope of the present program, the interrelation of the experimental data explaining as far as possible the mechanism of the action of antimony required a certain amount of interpolations to be made. Yet, we have done our utmost to give an unbiased description of the observed phenomena.

3.2. THE EFFECTS OF ANTIMONY

Three distinct effects of antimony positively influencing the behaviour of the positive electrode were identified. These effects were visible with:

(a) the first cycle capacity and the subsequent apparent active mass utilization ($Ah \cdot g^{-1}$) (Antimony effect 1);

(b) the early failure of a variable proportion of Sb-free electrodes with drastic capacity loss within 20 - 25 cycles (Antimony effect 2);

(c) the variable shorter overall lifetime of Sb-free electrodes (Antimony effect 3 and LODEF effect).

Effect Sb (1) depresses the active mass utilization by a few percent and could be possibly neglected.

Effect Sb (2) is more critical because a variable proportion of Sb-free electrodes fail early during cycle life. This proportion is dependent on the curing conditions. This early failure reflects a particular susceptibility of Sb-free electrodes towards variations in process parameters, parameters which are not critical when Sb is present in the grid alloy.

Effect Sb (3), i.e. the lifetime factor, represents approximately 30 to 34% less Ah life with flat and thin plates, and could be accepted if one considers the compensatory benefits of lower corrosion and lower maintenance of Sb-free systems.

3.3. THE EFFECTS OF ANTIMONY DURING THE CURING PROCESS

The curing process of the positive battery paste is an important step in the preparation of the positive electrode.

The paste, a mixture of tetragonal PbO, fine partially oxidized Pb-powder, basic lead sulfates ($3PbO \cdot PbSO_4 \cdot nH_2O$) and water, is pasted with a temperature of ~30 - 35°C and a pH of ~9.6 to 10.0 onto the lead alloy grid.

The subsequent curing process produces the "setting" and transformation of the paste from a wet plastic slurry into a rigid porous mass, the parallel oxidation of the free lead into hydrated and carbonated reaction products and also very important, the binding of the mass to the grid. The curing process also causes a water loss up to 10%, during the exposure to H_2O-unsaturated air between the pasting and final drying processes. This water loss can induce a macroscopic shrinkage of the mass and cracks could appear if the curing process has not reached the stage where sufficient strength is assured.

The observed effects of antimony during the curing process are limited to the grid-paste interface. The antimony is present as a metal or as an alkaline corrosion product (possibly Sb_2O_3) and shows a reduced mobility for migration into the bulk of the paste.

The following influences of antimony have been observed with the above described curing process:

- antimony produces an improved adhesion of the cured paste to the grid metal, the strength of the resulting metal-paste bond being equal or superior to the bulk paste-paste bond strength;

- antimony causes the reduction, change in nature and/or suppression of the corrosion of the grid alloy in the alkaline (pH 9.6 - 10.0) environment created by the wet paste of PbO and $3PbO \cdot PbSO_4 \cdot nH_2O$.

As possibly two of the three effects of antimony on the cycling behaviour of the electrode have been traced to curing conditions, we investigated the relevant phenomena in more detail.

3.3.1. ADHESION OF THE CURED ACTIVE MASS ON DIFFERENT GRID ALLOYS

The adhesion of the cured, unformed active mass to the grid metal containing antimony is markedly stronger than on e.g. a CaSn grid which underwent a regular, low temperature curing process.

The failure analysis concerning the antimony effect Sb^{II} - early failure has revealed that the principal damage in such samples is the delamination of the active mass from the grid, i.e. the formation of a thin 1 - 2 µm gap between the grid and the active mass observable already after formation.

This early failure pattern with antimony-free positive electrodes is very noxious as it conditions the entire behaviour of a battery if one or more electrodes randomly show a drastic capacity loss.

A certain amount of investigation has therefore been devoted to a better understanding of the curing phenomena and the correlation between the curing process and the early failures during cycling. No unambiguous correlation was found but,nevertheless, a number of critical parameters were readily discerned.

In the absence of any simple and rigorous testing method for determining the adhesion of the active mass to the grid, we simply broke the mass pellets from the grid frame with a pointed tool and observed the resulting grid surfaces.

The results obtained are shown in Fig. 25 and Table 17.

TABLE 17

GRID SAMPLE	ALLOY	CURING PROCESS	ADHESION	SHRINKAGE FRACTURES	OXIDE	Sb^{II} EFFECT EARLY FAILURE
1	7 Sb	DELCO-1+2	excellent	none	Barton	-
2	CaSn	DELCO-1+2	excellent	none	Barton	absent
3	7 Sb	DELCO-3	good	none	Barton	-
4	CaSn	DELCO-3	good	none	Barton	absent
5	7 Sb	BG - 13th batch	good	none	Ball-mill (new)	-
6	CaSn	BG - 13th batch	bad	none	Ball-mill (new)	present (~20%)
7	7 Sb	BG - 12th batch	good	numerous	Ball-mill (old)	-
8	CaSn	BG - 12th batch	bad	numerous	Ball-mill (old)	present (100%)
9	7 Sb	BG - 1st batch	good	(?)	Ball-mill (new)	-
10	CaSn	BG - 1st batch	good	(?)	Ball-mill (new)	present (25%)
11	7 Sb	SONNENSCHEIN (industrial)	medium	numerous	Ball-mill	-
12	CaSn	SONNENSCHEIN (industrial)	medium	numerous	Ball-mill	present (~80%)
13	5.5 Sb	PRESTOLITE (industrial)	good	numerous	Barton	-
14	3.3 Sb	PRESTOLITE (industrial)	good	numerous	Barton	-
15	CaSn	PRESTOLITE (industrial)	bad	numerous	Barton	present (~100%)

One immediately notices the varying degree of active mass adhesion. In view of the observed failure mechanism, such adhesion is welcome.

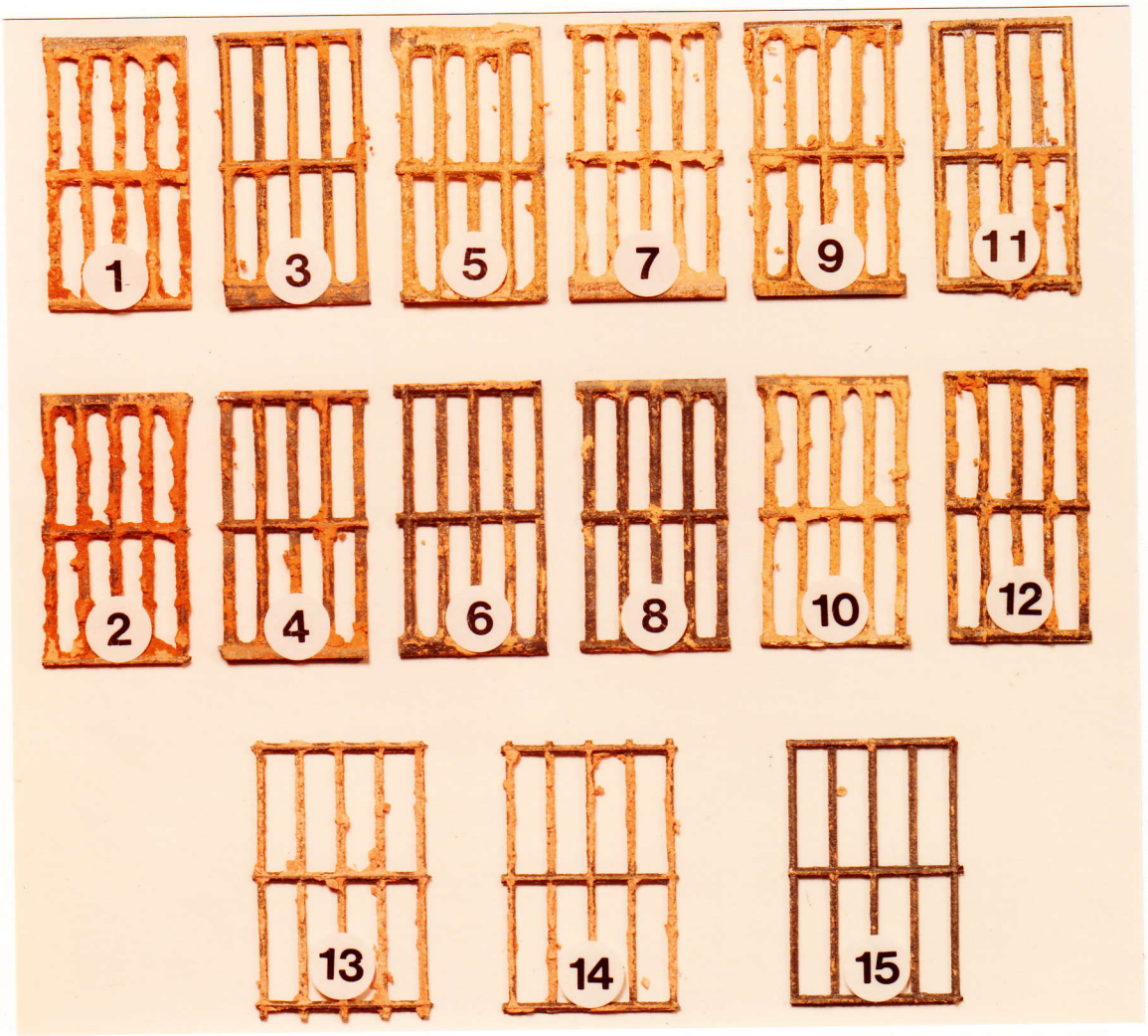

Fig. 25 Differences of active mass adhesion after curing (see table 17 for explanations).

Experiments established a certain correlation between the degree of adhesion and the chance of observing early failures in cycle life.

This correlation holds for:

- grids containing variable quantities of antimony (see Nrs 1, 3, 5, 7, 9, 11, 13, 14) and
- grids containing no antimony but treated with a particular curing process (DELCO-GM Nr. 2 and 4);

where with all the tested electrodes early failures were never observed.

The degree of adhesion observed and shown in Fig. 25 crudely describes one important set of the conditions required to avoid early failures. In fact,

- grids containing no antimony, showing bad adhesion (as Nr 6) but pasted with a mill-fresh oxide paste (see oxide characterization Ball-mill oxide Batch 13) and showing no shrinkage fractures induced during curing, are practically without early failures.

Whereas,

- grids containing no antimony, showing bad adhesion (Nr 8) pasted with an aged Ball-mill oxide paste (see oxide characterization Ball-mill oxide Batch 12) and presenting numerous curing induced shrinkage fractures, are plaqued by a variable degree (80% to 100%) of early failures.

This would indicate that the shrinkage fractures also play a critical, but not exclusive, role in the appearance of early failures.

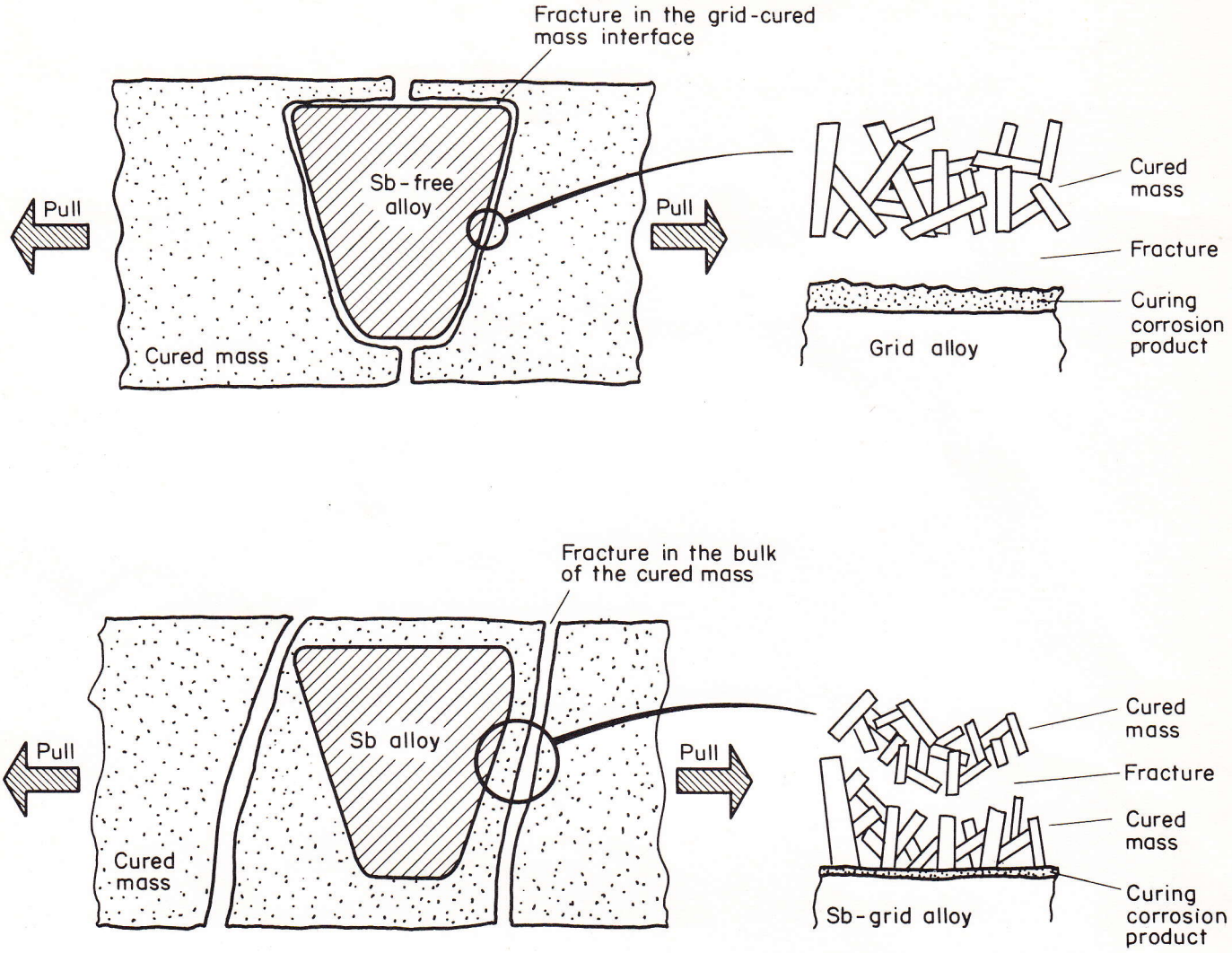

Fig. 26 Fracture pathways during the delamination of cured mass from Sb and Sb-free grids.

The previous experiments gave direct evidence for an improved adhesion of the mass already after curing with antimony alloy grids.

The schematic fracture lines during delamination of the active mass from the grid are shown in Fig. 26.

One notices the predominant fracture path occurring through the grid-cured mass interface with Sb-free grid electrodes, whereas the fracture is through the bulk of the active mass with Sb-grid electrodes. Several experiments were thus performed to isolate the interaction mechanism between the cured mass and the grid surface, and the related improved bonding when Sb is present.

We recall that the binding in this interface occurs:

- at pH 9.6 - 10.0 (equilibrium between Pb^{2+} and $HPbO_2^-$),
- in presence of air (oxygen and CO_2) and water,
- at a temperature between 35° and 55°C.

The investigations required: a detection of the quality and, if possible, quantity of the interface compounds and a verification of the improved bonding by adding an antimony source in this particular region.

A pronounced tarnishing of CaSn grids during the curing process was noticed. The respective Sb alloy grids revealed on the contrary only a very tenuous tarnishing reaction. Literature data indicated that Sb present in the alloy (see Gmelin Lead (B1), p.47) or the addition of a Sb compound prevents the oxidation of lead in neutral or alkaline solutions.

To detect the quality and quantity of interface products, we carried out the experiments described below.

Experimental conditions

In order to analyze the grid reaction product only and not similar products originating from the free lead or the oxide of the paste, bare grids of the type 7%, 4.5%, 2.7% Sb, CaSn, PbCa (binary) and pure Pb were immersed, in separate vessels, into the surnatant liquid of a settled positive paste-water suspension.This liquid simulated the environment of the wet paste without unduly contaminating the grid surface with extraneous products.

The immersed grids were then submitted to the curing temperature cycle of 48 h - 45°C and 24 h at 55°C, and then extracted and dryed for 18 h at 55°C in air.

After this treatment, the bare grids containing antimony showed only interference color thick oxides whereas CaSn, PbCa and pure Pb grids showed a grey reaction coating.

In situ X-ray analysis of the surface revealed:

- with 7% and 4.5% Sb grids
  minimal oxidation; reaction product $PbO_{(t)}$ → (good bond)
- with the 2.7% Sb grid
  increased oxidation; reaction product $PbO_{(t)}$ +
  appearance of the d: 3.067 Å peak of $PbO_{(0)}$ → (good bond)
- with CaSn, PbCa and pure Pb
  strong oxidation; reaction products now predominantly $PbO_{(0)}$ (daughter product of decomposed fine $Pb(OH)_2$) → (poor bond); also noticeable are lines of $PbO \cdot 0.33\ H_2O$ and $6PbCO_3 \cdot 3Pb(OH)_2 \cdot PbO$.

This indicates a higher reactivity, but nevertheless a lesser bond strength of Sb-free surfaces in the curing environment. The fact that $PbO_{(0)}$ is present on the surface, the daughter product of dehydrated fine $Pb(OH)_2$ comes somewhat as a surprise. The formation of $PbO_{(0)}$ indicates that the original Pb-hydrates are of very small crystal size, i.e. low cohesive strength (see PETERSEN, J. Am. Chem. Soc. 63 (1941) 2617/20).

In parallel with the above solution of pure paste-water suspensions, tests with soluble antimony species were also carried out. In these experiments, a paste slurry containing 0.7% w/w Sb_2O_3 was suspended in distilled water. In the surnatant clear liquid, pure lead sheets were immersed. Duplicate tests confirmed the inhibition of lead corrosion in a curing environment by the presence of Sb as metal or as Sb_2O_3 (dissolved). The X-ray diagrams of the relative surfaces revealed practically no corrosion reaction products when Sb_2O_3 was present, whereas with Sb-free curing, $PbO_{(0)}$ and $PbO \cdot 0.33\ H_2O$ were noticed (see Fig. 27). (The X-ray diagrams were made under identical conditions by using the lead d = 2.85 Å peak as internal reference.)

The inhibition of lead oxidation by Sb_2O_3 was also noticed by other experimenters (RITCHIE-ILZRO report LE-82/1971). This hampers the introduction of Sb_2O_3 into the positive electrode via its addition to the paste as the oxidation of the free Pb in the oxide mix is inhibited.

The improved adhesion of active mass paste in presence of antimony was also verified by coating the surface of a lead sheet with a thin layer of a Sb_2O_3 (applied as water suspension). As expected, the subsequent application of paste, curing and drying, revealed a much better adhesion of the mass on lead with a Sb_2O_3 coating. See also Fig. 28.

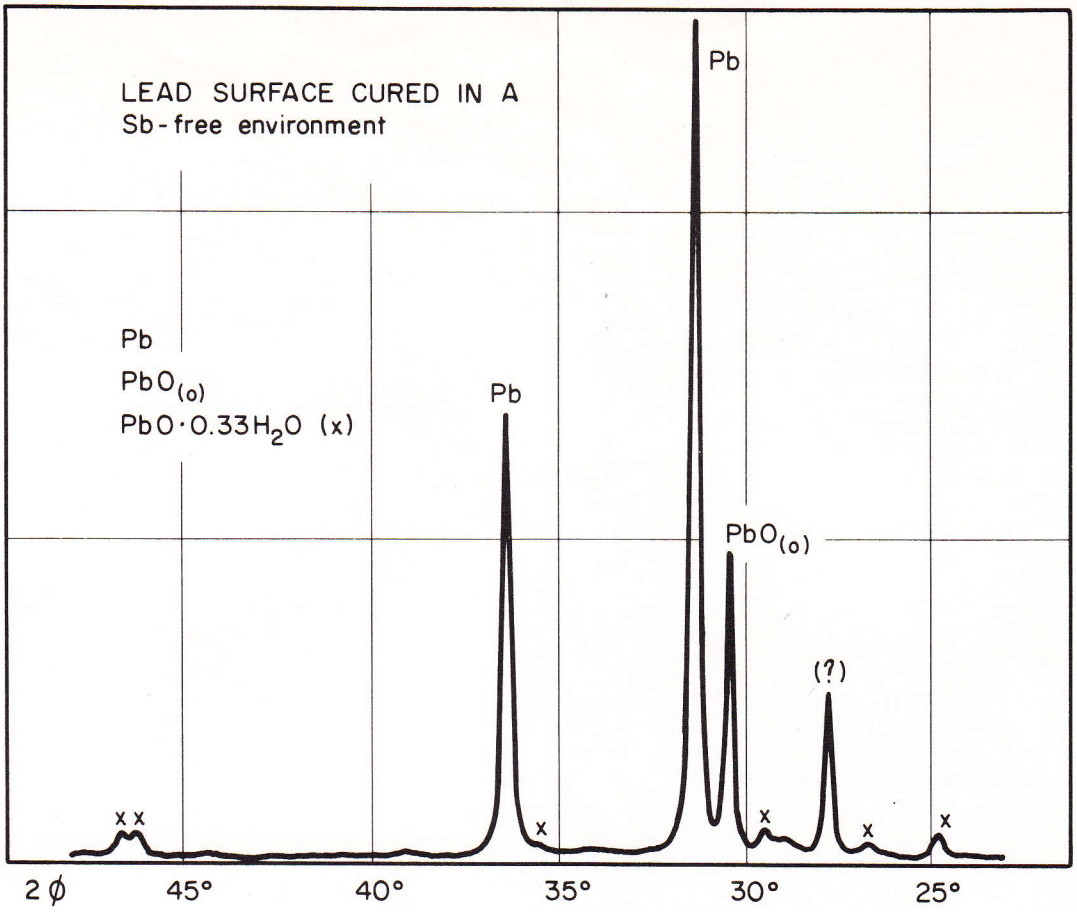

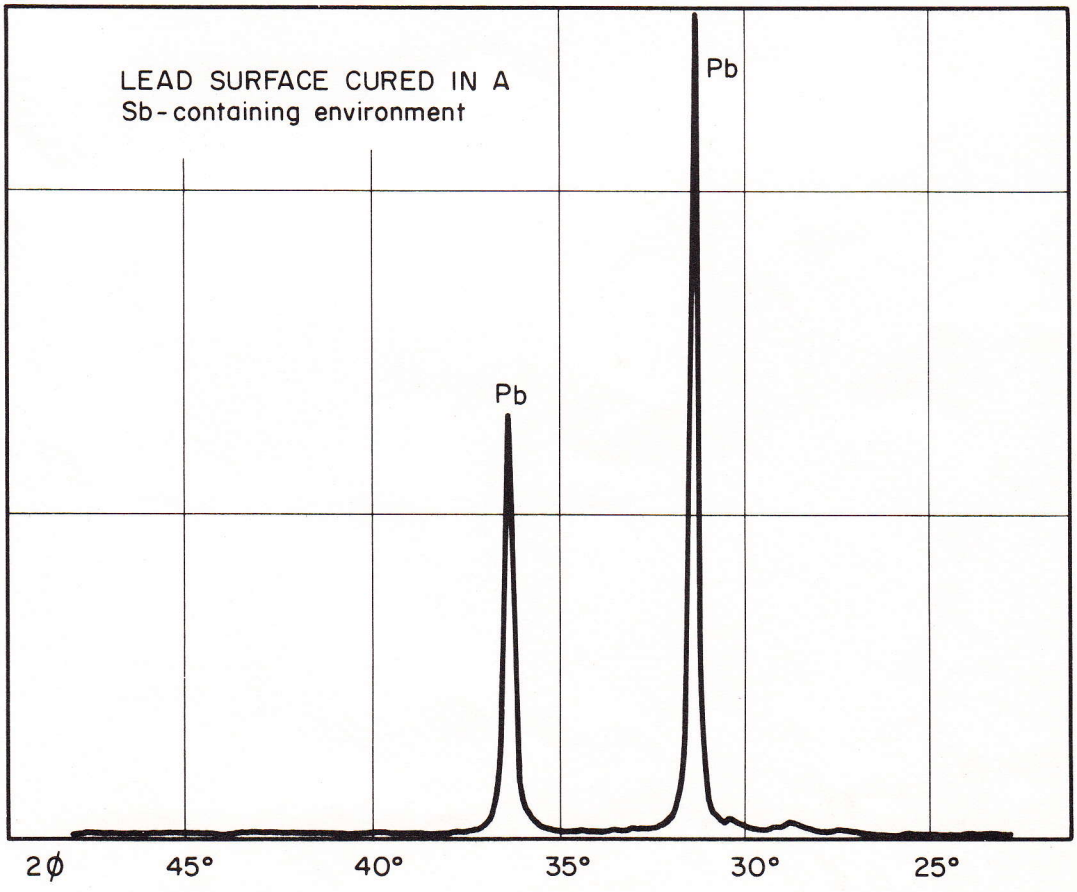

Fig. 27 X-ray diffractograms of lead surfaces exposed to the curing environment with or without Sb species present.

The exact mechanism of the antimony-promoted bonding in the cured state is not yet clear. In similar experiments involving Sb_2O_3-PbO paste mixes, we observed a rapid change of the rheological properties of the paste, i.e. an initial stage of increased fluidity followed by a rapid stiffening of the paste. This could indicate a possible interaction between the Sb_2O_3 and the PbO + $3PbO \cdot PbSO_4 \cdot nH_2O$ mixture.

The technique of improving the bonding in presence of a Sb_2O_3 coating on the grid was tested on a set of CaSn electrodes. The obtained positive result, i.e. improved adhesion after curing, was counterbalanced by a Sb_2O_3-caused irregular active mass formation which led to a rapid capacity loss (see Sb^{II} effect experiments).

3.3.2. POSSIBILITIES TO IMPROVE THE "AFTER CURING" ADHESION WITHOUT ADDITION OF ANTIMONY

In the experiments with cast CaSn electrodes, which were pasted and cured with a proprietary procedure by DELCO-GM to a tetrabasic mass, an excellent adhesion of the active mass to the grid member was observed. The high temperature curing process employed promotes the bond of the cured mass to the grid and an X-ray analysis of the grid surfaces did not reveal the presence of either $PbO_{(0)}$ nor $PbO \cdot 0.33\ H_2O$. (NB: The analysis of the grid surface was rendered difficult by the interferences caused by the adherent active mass. The analysis of the real interface products was ensured by choosing the X-ray analysis parameters (accelerating voltage and current) so as to detect metallic lead on the diffractogram, i.e. all material down to the grid surface was participating in the diffraction pattern.) S.E.M. analysis revealed the existence of an oxidation layer but this showed a good interlock with the large $4PbO \cdot PbSO_4$ needles. Subsequent to these observations, the Sb^{II} effect, i.e. early failures, was not observed with DELCO-GM

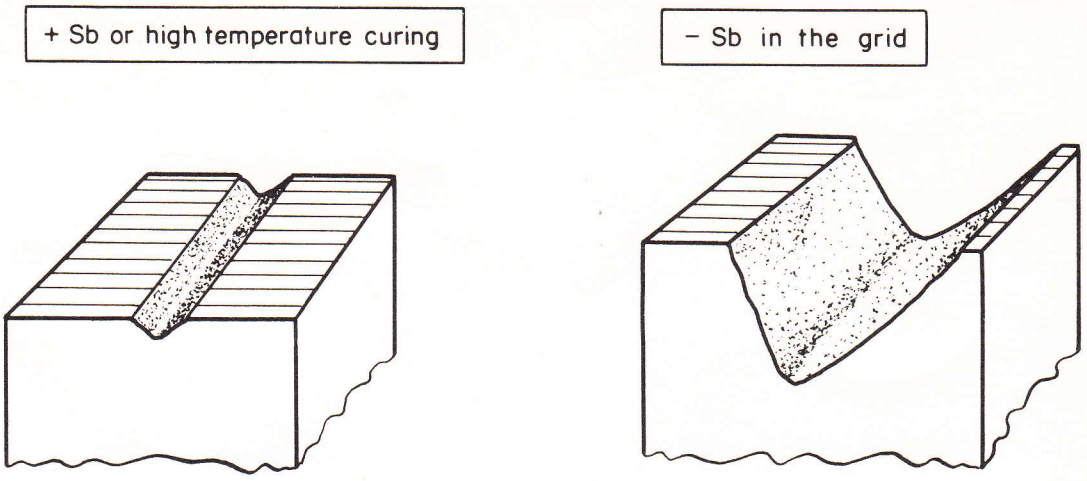

Pellet of cured mass broken from the grid

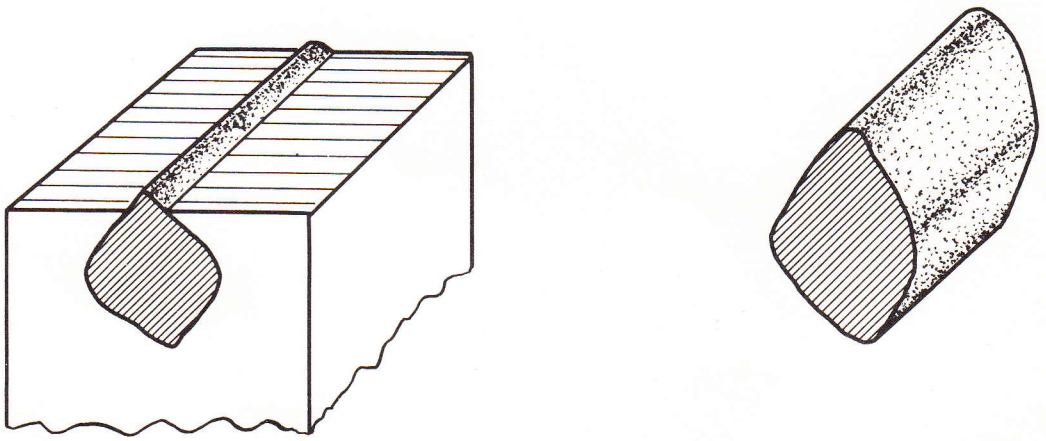

Relative grid portion with variable fracture path

Fracture path through cured mass

Fracture path through grid-cured mass interface

Fig. 29 Fracture paths after curing as related to the S.E.M. analysis of the interfaces.

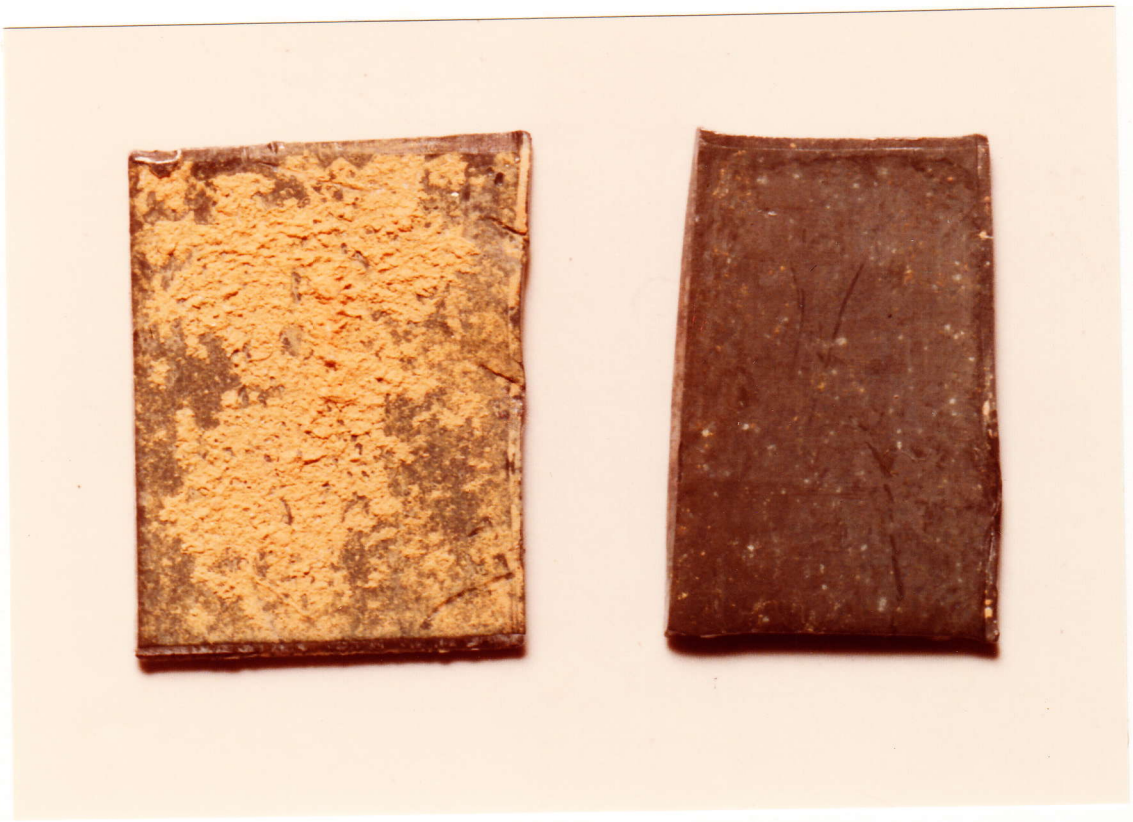

Fig. 28 Influence of Sb species on the adhesion of cured active mass on pure lead.

Left: good adhesion with an intermediary Sb_2O_3 coating.

Right: bad adhesion on the clean Pb surface.

cured electrodes. The Sb^{I} effect is noticed with the DELCO-1 and DELCO-2 effect but not with the DELCO-3 set.

3.3.3. SEM ANALYSIS OF FRACTURE SURFACES RELATED TO THE DIFFERENTIAL ADHESION OF THE CURED MASS TO THE GRID

In order to visualize the differentiated bonding between Sb and Sb-free grids, the cured active mass was split along the specific weakest path from the grids (see schematic view in Fig. 29).

Fig. 30 shows the pellet surface as split from the Sb alloy grid of Fig. 31.
Only a very small amount of the fracture path passes through the interface grid-cured mass.

Fig. 31 reveals the good adherent residues of cured mass on the two grid members.

Fig. 32 reveals the details of this mass residue.

Fig. 33 shows the pellet surface as split from the CaSn alloy spine of Fig. 34.
The fracture path initiated in the active mass (left part) proceeds at the interception of the grid-cured mass interface through the latter, weaker bond region.

Fig. 34 reveals the practically mass devoid CaSn grid spine.

Fig. 35 shows the surface of the spine with the corrosion product $PbO_{(0)}$ ex $Pb(OH)_2$, $PbO \cdot 0.33\ H_2O$, $6PbCO_3 \cdot 3Pb(OH)_2 \cdot PbO$ formed during curing. This layer does not bond well to the cured mass, and results in a structurally weak interface.